Comparison of Beidou Autonomous Navigation Performance using the SRP model and onboard Accelerometers

Jing Qiao[1,2,*], Guochang Xu[3], Wanke Liu[4], Wu Chen[1]

[1] Department of Land Surveying and Geo-Informatics, Hong Kong Polytechnic University, Hong Kong, China

[2]Institute of Geodesy and Photogrammetry, ETH Zurich, Switzerland

[3] Institute of Space Science, Shandong University, Weihai, China

[4] School of Geodesy and Geomatics, Wuhan University, Wuhan, China

* Correspondence: jing.qiao@connect.polyu.hk

Abstract The Autonomous Navigation (AutoNav) mode of a Global Navigation Satellite System (GNSS) utilizes Inter-Satellite Links (ISLs) to maintain satellite operations without the service from the ground control segment. The newly launched Beidou satellites are capable of conducting ISLs for orbit determination to improve their autonomy, integrity, reliability, and robustness. However, the satellite orbit errors can increase over time due to various force model errors, particularly that of Solar Radiation Pressure (SRP). Accelerometers onboard satellites can measure non-conservative forces directly and have been successfully used in satellite missions for gravity recovery and atmosphere study (i.e., GRACE, CHAMP, and GOCE). This study investigates the feasibility to use accelerometers onboard Beidou satellites to improve AutoNav accuracy and service span. The results show that in a simulated 180-day AutoNav period, the orbit accuracy with the aid of accelerometers is two times better than that of using ISL data only.

Keywords Beidou Navigation Satellite System; Autonomous Navigation; Solar Radiation Pressure; Accelerometer

1. Introduction

The concept of using ISL measurements to achieve GPS AutoNav without interfering with the operational control segment (OCS) has been proposed since the early 1980s. The first conceptual feasibility study of GPS AutoNav was conducted by the Aerospace Corporation [1]. The simulation study showed that GPS could keep navigation accuracy for 180 days with the use of inter-satellite ranging measurements only. The follow-on study by the Rockwell International and the Space Applications Corporation demonstrated its onboard implementation feasibility [2]. IBM further developed the AutoNav algorithm and included a measurement editing scheme to improve the robustness of the algorithm [3]. AutoNav simulation and brassboard testing activities for GPS Block IIR also confirmed the feasibility and laid a basis for the implementation of ISL [4]. The on-orbit validation of GPS IIR AutoNav showed that 2-6 m User Range Errors (URE) in the 15-day orbit arc could be achieved [5].

The Chinese Beidou Navigation Satellite System (BDS) will consist of 35 satellites for global coverage, including 5 Geosynchronous Earth Orbit satellites (GEOs), 3 Inclined Geo-Synchronous Orbit satellites (IGSOs) and 27 Medium Earth Orbit satellites (MEOs). Ranging measurement among the spacecraft has been proposed to overcome the problems related to the existing Beidou system [6], especially the lack of global coverage of the ground tracking network and the poor observation geometry for GEOs and IGSOs. The initial tests for BDS inter-satellite ranging have been carried out with five Beidou satellites launched in 2015. Several research groups have studied the performance of BDS AutoNav. Using

simulated ISLs with fixed bias of 8 cm, a cyclic bias of 5 cm, and measurement noise of 0.75 m, BDS AutoNav in 20 days could achieve 0.10, 0.60, and 0.20 m accuracy in orbit radial, horizontal direction, and URE, respectively [7]. Another study showed BDS AutoNav orbit accuracy could reach 3.0 m URE over 90 days, with ISL measurement noise of 1.0 m [8]. A combined orbit determination experiment using ISLs of BDS and ground tracking stations in China has also been conducted. The orbit determined with ISL data achieved 37-76% improvement in signal-in-space (SIS) range accuracy [9].

The dominant factors affecting AutoNav orbit accuracy are the unobservable rotational errors, including rigid body rotation and the earth orientation parameters (EOPs) prediction errors [3, 10, 11].

The rigid body rotation problem is induced by the fact that only ISLs which can maintain the relative distance between the satellites are used in the AutoNav mode. Without absolute observations to the external objects, such as the Earth or other celestial bodies, the AutoNav system cannot detect the drift of the whole constellation by a certain angle, leading to large spurious rotations. Thus, in the AutoNav mode, GNSS satellite orbit errors are mainly induced in the along-track and cross-track directions. A specific analysis of the observability issue is given in the previous literature [11]. One proposed method to mitigate this problem is using the predicted satellite angular elements from OCS to set up constraint equations in the AutoNav process [7, 12]. Therefore, accurate prediction of these elements is of vital importance for constellation rotation constraint. The orbit prediction accuracy depends on the initial orbital elements and the dynamic force models. With the long arc and high precision ground tracking observations in normal orbit determination mode, the initial elements should be accurately estimated, and the orbit can be extrapolated for a rather long period if the satellite perturbation forces can be well modeled. However, not all of the

satellite perturbations can be accurately modeled at present. Satellite perturbations can be divided into conservative and non-conservative ones. For conservative forces, such as the earth non-spherical gravitational perturbations, third-body attractions, and tide effects, current models are capable of correcting them precisely. However, the non-conservative forces, particularly SRP, are still difficult to model accurately. Although various SRP models have been proposed, such as the analytical models of ROCK [13] and G2A [14], the empirical models of ECOM [15, 16] and GSPM [17] and the semi-analytical adjustable box-wing model [18], SRP model error is still the dominant perturbation error affecting GNSS satellite orbit determination and prediction accuracy.

Various ways have been investigated to reduce the constellation rotation problem. Using anchor stations [19] is the simplest way to control the rotation of the constellation. However, links have to be established between the earth and the satellite system, which is not fully autonomous. Using an onboard camera to observe the planet surface for landmark tracking or image motion tracking is adopted for AutoNav of planetary flybys or missions too far away from the earth, but not for GNSS due to its low accuracy [20].

Onboard accelerometers can accurately measure the non-conservative forces and have been successfully used in missions of gravity field recovery and atmosphere study, and their role in precise orbit determination for low earth orbit (LEO) satellites has also been investigated [21, 22]. Using accelerometers and ISL data for GPS satellites orbit determination have been proposed by Ash [23].

Simulation study to evaluate the accelerometer performance in Beidou AutoNav mode has also been carried out [24]. Using accelerometers to measure the non-conservative forces can achieve better orbit accuracy, compared with using the empirical SRP force model. However, in this simulation, the orbits of satellites were simulated simply using orbit

integration with given force models; then the ISL data were simulated using these 'perfect' orbits and their dynamic information was accurately known. Therefore, the results from this study may be too optimal, compared with a real situation.

In this study, we compare the performances of Beidou AutoNav with onboard accelerometers and empirical SRP model. In data generation, we use the real GNSS satellite orbits from IGS to simulate ISL data. The accurate dynamic information of these orbits is unknown as in the actual situation, which will provide more reliable results than the previous study. Moreover, more rigorous data simulation and verification process are proposed to evaluate the orbit determination accuracy. The paper is organized in the following way. The AutoNav observation equations, error models, AutoNav orbit determination methods, as well as a remedy to deal with the EOPs prediction errors, are described in section 2. Then, detailed data simulation and verification process are presented in section 3. Section 4 shows the simulation results and accuracy analysis with the two cases. The conclusions and recommendations for future work are given in section 5 and section 6, respectively.

2. ISL observation equation, error model and AutoNav algorithm

For the two AutoNav modes, when only ISL data are used, the reduced ECOM which has shown its advantages of efficiency and accuracy in orbit determination of Beidou IGSOs and MEOs [25] is used to estimate the vehicle surface SRP; when the onboard accelerometers are used to measure the non-conservative forces directly, corresponding error model is needed to calibrate the accelerometer raw observations. This section describes the ISL observation equation, accelerometer data and its calibration model, as well as the AutoNav algorithms for two modes.

2.1. ISL observation equation

The Time Division Multiple Access (TDMA) mode is used to generate inter-satellite range observations. The ISL data are generated and satellite orbits and clock errors are updated every 15 min, and each 15-min interval is called an AutoNav frame. A 1.5-sec time slot is assigned to each satellite sequentially since the start of a frame. The satellite transmits signals to all possible directions in its corresponding slot, and other visible satellites receive the signals and derive the crosslink pseudo-ranges. A sketch of the measurement geometry of the ISL data is shown in Figure 1. The centralized AutoNav system collects and processes all the measurements on one central satellite [26], and it can provide higher overall accuracy for the satellite ephemerides and clocks than a distributed system. Thus it is adopted in this research. The basic observation equations, orbit and clock determination equations are described below.

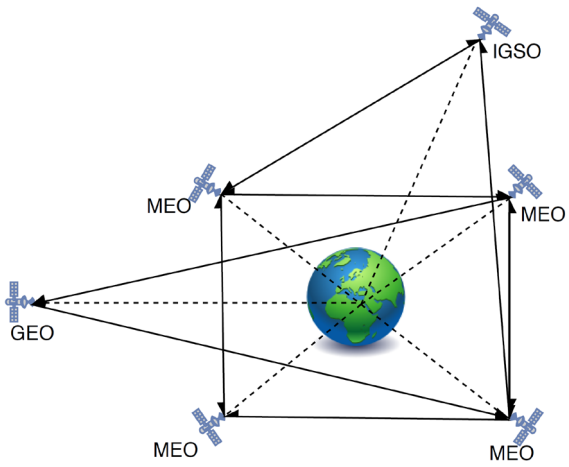

Fig. 1. A sketch of the measurement geometry of the ISLs

The crosslink ionosphere-free pseudo-range measurements corrected by relativistic effects, satellite and receiver antenna phase center offsets, and so forth, between two satellites are denoted as:

$$\begin{aligned}\rho_{ij} &= L_{ij} + c\delta_{j1} - c\delta_{i1} + \varepsilon_{ij} \\ \rho_{ji} &= L_{ji} + c\delta_{i2} - c\delta_{j2} + \varepsilon_{ji}\end{aligned} \tag{1}$$

where ρ_{ij} and ρ_{ji} are the pseudoranges between satellites *i* and *j*, L_{ij} and L_{ji} represent the geometric distances between satellites at signal sending and receiving epochs in opposite directions, c denotes the speed of light, $\delta_{i1,}\delta_{j1,}\delta_{i2,}\delta_{j2}$ are satellite clock errors at each epoch, and $\varepsilon_{ij,}\varepsilon_{ji}$ are measurement noises and systematic biases. By subtracting these two equations, the time synchronization equation can be obtained; adding these two equations and applying linearization, the orbit determination equation can be deduced.

2.1.1. Time synchronization equation

$$\rho_{ij} - \rho_{ji} = L_{ij}^{0} - L_{ji}^{0} + cA_j\vec{X}_j(\mathrm{t}_0) - cA_i\vec{X}_i(\mathrm{t}_0) + \varepsilon_{ij} - \varepsilon_{ji} + \delta L_{ij} - \delta L_{ji} \tag{2}$$

where

$$\begin{aligned}A_k &= (2 \quad t_{k1} + t_{k2} - 2\,\mathrm{t}_0), \quad \mathrm{k} = \mathrm{i}, \mathrm{j} \\ \vec{X}_k(\mathrm{t}_0) &= (a_0^k \quad a_1^k)^{\mathrm{T}}, \qquad \mathrm{k} = \mathrm{i}, \mathrm{j}\end{aligned} \tag{3}$$

$t_{k1,}t_{k2}$ are the signal sending and receiving epochs, t_0 is the initial epoch of one AutoNav frame, a_0^k, a_1^k are satellite clock bias and drift rate, L_{ij}^0, L_{ji}^0 represent the computed distances using the predicted satellite positions, and $\delta L_{ij}, \delta L_{ji}$ denote the differences between the computed and true distances. Though accurate satellite clock errors are not known, the clock errors should be considered and taken from predicted values while predicting satellite positions. In this way, δL_{ij} and δL_{ji} can be ignored in the clock error updating process [27].

2.1.2. Orbit determination equation

$$\begin{aligned}\rho_{ij}+\rho_{ji}=L_{ij}^{0}+L_{ji}^{0}+\frac{\partial\rho}{\partial\vec{X}_i(\mathrm{t}_{i1})}\delta\vec{X}_i(\mathrm{t}_{i1})+\frac{\partial\rho}{\partial\vec{X}_j(\mathrm{t}_{j1})}\delta\vec{X}_j(\mathrm{t}_{j1})\\+\frac{\partial\rho}{\partial\vec{X}_i(\mathrm{t}_{i2})}\delta\vec{X}_i(\mathrm{t}_{i2})+\frac{\partial\rho}{\partial\vec{X}_j(\mathrm{t}_{j2})}\delta\vec{X}_j(\mathrm{t}_{j2})+\mathrm{c}\,\delta\mathrm{t}+\varepsilon_{ij}+\varepsilon_{ji}\end{aligned} \tag{4}$$

where

$$\begin{aligned}&\delta t=\delta_{j1}-\delta_{j2}-\delta_{i1}+\delta_{i2}\\&\delta\vec{X}_k(\mathrm{t}_{kn})=\psi(\mathrm{t}_{kn},\mathrm{t}_0)\delta\vec{X}_k(\mathrm{t}_0),\ k=i,j\ ;\ n=1,2\end{aligned} \tag{5}$$

$\psi(\mathrm{t}_{kn},\mathrm{t}_0),\ k=i,j\ ,\ n=1,2$ are the state transition matrices, and $\delta\vec{X}_k(\mathrm{t}_0),\ k=i,j$, denote the state correction vectors at the initial epoch, including satellite position, velocity, and dynamic parameters, e.g., SRP parameters or accelerometer calibration parameters; $\delta\vec{X}_k(\mathrm{t}_{kn}),\ k=i,j\ ,\ n=1,2$ are the propagated state correction vectors at the observation epochs. Satellite state and state transition matrix of each epoch can be derived by integrating its motion and variation equations. The linearization error in (4) is negligible in AutoNav and does not show here.

2.2. Accelerometers and error model

The general concept of ultra-sensitive space accelerometer is based on the accurate electrostatic suspension of a proof mass. The accelerometer outputs are derived from the electrostatic forces exerted on the mass to maintain its motionless with respect to the satellite [28]. The electrostatic forces are corresponding to the non-gravitational perturbations on the surface of the satellite. The characteristics of the three gravity satellite accelerometers are listed in Table 1, Y and Z refer to two sensitive axes in the Satellite Reference Frame (SRF)[29].

Table 1 The main characteristics of the CHAMP, GRACE and GOCE accelerometers

Mission	CHAMP	GRACE	GOCE	Unit
Measurement range Y, Z	$\pm 10^{-4}$	$\pm 5\times 10^{-5}$	$\pm 6.5\times 10^{-6}$	ms^{-2}
Specified resolution Y, Z	3×10^{-9}	10^{-10}	2×10^{-12}	$ms^{-2} / Hz^{1/2}$
Measurement range X	$\pm 10^{-4}$	$\pm 5\times 10^{-5}$	$\pm 6.5\times 10^{-6}$	ms^{-2}
Specified resolution X	3×10^{-8}	10^{-10}	2×10^{-12}	$ms^{-2} / Hz^{1/2}$

Taking the data of GRACE A satellite as an example of error analysis, the accelerometer Level-1A data are dominated by the so-called peak effect, twang effect and thruster events. The first two effects are not caused by the surface forces and would contribute to the measurement error budget. Their influences are negligible at low frequencies, and the low-pass filtered Level-1B data are almost unaffected. The thrust events are part of GRACE angular control system, and they can map into the measured linear accelerations in two cases: the proof mass is not ideally placed at the satellite center of mass; a misalignment exists between the thrusters of a thruster pair, and the thrust forces or reaction times are different. In the second case, the induced acceleration affects satellite motion, and it is necessary to be measured, though much smaller, which is similar to trajectory maintaining thrust forces for the GEOs/IGSOs. In the first case, the effect in the measurement is not caused by an actual acceleration on the satellite and should be mitigated. The mass trim assembly manages to keep the satellite center of mass within 100 μm to the proof mass and the acceleration due to angular motion is smaller than accelerometer or K-band measurement errors for GRACE satellites [30].

As with GRACE, we assume that the first two non-surface effects can be effectively eliminated by preprocessing for Beidou satellites. The attitude of Beidou satellites are actively controlled to maintain the +z-axis orienting towards the earth, and the IGSOs/MEOs have to rotate about the z-axis to keep the y-axis perpendicular to the earth-sun-satellite plane in their yaw-steering (YS) mode. To analyze the angular motion effect on the accelerometer, we also assume that the offset of the satellite mass center to the proof mass stays within $r =$ 100 μm. The z-axis rotates once in one satellite revolution period, e.g., 13 h for MEO satellite, the inertial angular velocity is $\omega = 1.34 \times 10^{-4}\mathrm{rad/s}$ and the centripetal acceleration $r\omega^2$due to proof mass offset is less than $1.80 \times 10^{-12}\mathrm{m}/s^2$. It can be seen that the effect on accelerometers due to attitude control to keep +z-axis pointing to the earth is smaller than the specified accuracies in Table 1. The IGSOs/MEOs are generally in their YS mode and switch to orbit-normal (ON) mode, yaw angle=0, when the sun elevation angle falls below approximately 4°. Although we do not know the exact switch process, it is expected that the maximum yaw rate is $0.6^{\circ}/s$. If the maximum rate is employed, only 10 s would be taken to finish the attitude switch and the induced centripetal acceleration in the accelerometer would be $1.0 \times 10^{-8}\mathrm{m}/s^2$ [31]. The centripetal acceleration is much smaller in nominal mode and thus ignorable. Besides, some IGSOs/MEOs of Beidou-2 have abandoned the YS-ON mode and adopted a continuous YS mode, which might also be favored by Beidou-3. A YS model with yaw angle fitting accuracy of 3°during noon and midnight turn maneuvers has been proposed [32]. The modeled maximum yaw rates are $0.159^{\circ}/s$ and $0.085^{\circ}/s$ for MEOs and IGSOs respectively and the effects on the accelerometers are 7.7× $10^{-10}\mathrm{m}/s^2$and $2.2 \times 10^{-10}\mathrm{m}/s^2$. Furthermore, as the attitude control can be modeled, the angular effect on accelerometers may also be removed with to be known mass center and proof center offset r and the equation $r\omega^2$.

On the other hand, due to instrument measurement errors, the raw Level-1B data also need to be calibrated. The generally used calibration model contains an instrument scale factor and a bias in each direction, and it is expressed as

$$f_{new} = bias + scale \times f_{acc} \tag{6}$$

Based on the analysis of routinely estimated results, a recommendation is given for the scale and bias parameters to calibrate for the Level-1B accelerations of GRACE [33]. The recommended scale values are usually used directly in precise gravity recovery and no longer estimated [34]. The biases are modeled by quadratics over a long period and the accuracy is within a few percent. The expression for the bias recommendation is:

$$bias = c_0 + c_1(\mathrm{T_d} - \mathrm{T_0}) + \mathrm{c}_2(\mathrm{T_d} - \mathrm{T_0})^2 \tag{7}$$

where c_0, c_1, c_2 are the coefficients, and T_d, T_0 are Modified Julian Dates (MJD), T_d is the current time, T_0 is the reference time (53736 for a date after March 3, 2007).

2.3. Satellite autonomous orbit determination methods

Based on whether accelerometer data are used, two orbit determination methods are implemented for the simulated BDS constellation. One is using only the ISLs and the other is using ISLs together with the accelerometer data. The reference frames and common dynamic models used in both cases are listed in Table 2. The detailed AutoNav processes of these two methods are described below.

Table 2 Reference frames and dynamic models

Reference Frames and Orbit Models	
Inertial frame	ICRF at J2000.0
Terrestrial frame	ITRF2008
Precession model	IAU 2000 Precession theory
nutation model	IAU 2000R06 Nutation theory
EOPs	Polar motion & UT1 from IERS C04 series
Geo-potential (static)	EGM2008 model 12×12
Solid earth tides	applied according to IERS 2010 [35]
Third-body	Sun, Moon, Jupiter, Venus, Mars as point masses
Ephemeris	JPL DE406
Numerical integration	Runge-Kutta 4, step = 60.0s

2.3.1. ISL observations only

In the case that only ISL observations are used, the SRP parameters of the reduced ECOM need to be estimated. Five SRP parameters and satellite initial position, velocity vectors are updated in each AutoNav frame using the derived orbit determination equation through the Extended Kalman Filter [36]. In the meantime, satellite clock biases and drifts are updated with the derived clock measurement through a separate Kalman Filter.

The satellite orbit in each frame is obtained by orbit integration with the equation of motion

$$\ddot{\mathbf{r}} = -GM\frac{\mathbf{r}}{r^3} + f_0(t,\mathbf{r},\dot{\mathbf{r}}) + f_{SRP}(t,\mathbf{r},\dot{\mathbf{r}},p_1,p_2,\cdots,p_5) \quad (8)$$

where $\mathbf{r}$ is the geocentric position of the satellite mass center and p_i $(i = 1,2,\ldots,5)$ are the SRP parameters [16]. The first item on the right-hand side of the equation represents the Earth central force, the second one denotes the perturbations than can be well modeled, and the third one is the SRP force represented by the reduced ECOM.

2.3.2. ISL and accelerometer data

With a set of accelerometers to measure the non-conservative forces, the SRP model is not needed under this circumstance. The accelerometer measurement biases should be estimated instead due to its measuring error. Considering the varying pattern of the biases, we set up a linear model in each direction of SRF $Bias_i = k_i dt + b_i \ \ (i = 1,2,3)$, where dt is the time difference between the current and a reference epoch. These 3×2 accelerometer parameters are updated together with satellite initial position and velocity. The constellation rotation constraints and updating methods for satellite state vectors and clock errors are the same as those of the first case. The initial values of the accelerometer bias coefficients are set as true values of the model at the start of AutoNav.

The satellite orbit in each frame is obtained by orbit integration with the equation of motion

$$\ddot{\mathbf{r}} = -GM\frac{\mathbf{r}}{r^3} + f_0(t,\mathbf{r},\dot{\mathbf{r}}) + f_{SRP}^o + f_{SRP}^c(t,k_1,k_2,k_3,b_1,b_2,b_3) \quad (9)$$

where the first two items on the right-hand side of the equation are the same as those in equation (8). The items f_{SRP}^o and f_{SRP}^c stand for the observed SRP force by the accelerometer and the correction to the observed force to mitigate accelerometer measuring errors, respectively.

Comparing the expressions of f_{SRP} in equation (8) and f_{SRP}^c in equation (9), we can notice that the accuracy of the modeled SRP force in the first method depends not only the quality of SRP parameters but also on the satellite orbit $(\mathbf{r},\dot{\mathbf{r}})$, whereas, only the accelerometer calibration parameters affect the accuracy of the SRP correction in the second case.

2.3.3. EKF and constraint conditions

Two kinds of estimators can be used for satellite state and clock updating, one is the batch processing Least Squares Method (LSM), and the other is the epoch by epoch processing Kalman Filter. To realize real-time navigation, the Kalman Filter should be chosen. Due to the non-linearity of the satellite dynamic motion equation and orbit determination equation, the EKF is implemented in the AutoNav process. Satellite clock, position, velocity and dynamic parameters at the initial epoch of each ranging frame are updated with observations in the frame through the filters, respectively.

Appropriate conditions are established in the ephemeris filter to constrain the constellation rotation. For the constraint equation in the ephemeris filter, satellite orbit inclination i and right ascension of the ascending node (RAAN) Ω, predicted from the previous frame, are used to set up equality conditions. For GEOs, the orbit inclination is close to zero. Thus the second non-singular orbital elements $h = sini\ cos\Omega, k = sini\ sin\Omega$ are adopted to establish the equality conditions[7].

2.4. EOPs prediction error

As mentioned before, without ground contact, the EOPs are unobservable in AutoNav mode, and the predicted EOPs should be used in satellite AutoNav. However, the accuracy of current predicted EOPs may not satisfy the AutoNav requirement in a long service period. To reduce the effect of the prediction error, we first give an analysis of the roles of EOPs in AutoNav:

(1) Calculating the earth gravitational perturbation and derivatives in orbit integration process in the inertial reference frame (IF): the EOPs are used to transform the satellite state

vectors from IF to terrestrial reference frame (TF), so as to obtain the earth gravitational perturbation and derivatives using the earth potential represented by the Laplace equation in spherical coordinates; and then transform the perturbation and derivatives from TF to IF for orbit determination.

(2) Transforming the satellite orbits of AutoNav results from IF to TF for users on the earth.

To investigate the effect of predicted EOPs to AutoNav in these two aspects, we have conducted experiments with accurate and predicted EOPs. The accurate EOPs are the International Earth Rotation and Reference Systems Service (IERS) final products, IERS C04 series, and the predicted EOPs are the latest IERS bulletin-A weekly solutions on the starting day of AutoNav.

For the first aspect, the predicted EOPs have been adopted in the AutoNav process with SRP estimated. The AutoNav results are output in the IF, then transformed into TF with accurate EOPs and compared with the orbits obtained in the AutoNav using the accurate EOPs all through. The differences between these two sets of orbits are on an mm-cm level in the horizontal direction in 180 days and almost no difference is shown in the radial direction. These differences indicate that the EOP prediction errors only slightly affect the calculated gravitational perturbations on BeiDou satellites, and the AutoNav results are not deteriorated by the predicted EOPs.

Although the predicted EOPs have a slight effect on gravitational perturbations in orbit integration, the orbit can drift over time with increasing errors in the predicted EOPs, especially UT1, while transformed from the IF to TF. An AutoNav experiment estimating SRP has been done using the predicted EOPs and output the results in TF. Comparison with orbits determined using accurate EOPs shows that the orbit radial accuracies are the same, while a rapid increase over time is displayed in the horizontal orbit errors one month after the

starting epoch of AutoNav. The MEOs horizontal orbit accuracies are 2.5, 17, 36, 50, 56, and 80 m at the end of 1, 2, …, 6 months; horizontal orbit errors proportional to the radius are also shown for the GEOs/IGSOs. A remedy for the second aspect can be made with a two-step coordinate transformation if higher accuracy is needed by the users. Firstly, they can use the predicted EOPs which have been used in the AutoNav process to convert the AutoNav broadcast orbits from TF to IF; then, with accurate EOPs which can be estimated and predicted with other techniques (VLBI, SLR, DORIS) in real-time, the users will be able to transform the orbits from IF to TF for their usage. In this way, the satellite orbit will be free from EOP prediction errors in the final coordinate system transformation.

The orbit errors due to the use of predicted EOPs then mainly come from the earth gravitational perturbation and derivatives calculation, just mm-cm in the horizontal direction, and can be ignored. To simplify the experiment, we use accurate EOPs in this simulation study.

3. Data simulation and AutoNav

Since BDS has not yet realized its 35-satellite full constellation, some of GPS satellites were used in this study to represent MEOs of the future BDS. The studied AutoNav period is six months, and the ISL data were generated with IGS precise ephemerides of MEOs and simulated ephemerides of GEOs/IGSOs based on their available IGS precise orbits; the accelerometer data were simulated considering the modeled SRP forces and measurement errors. The data simulation and AutoNav were conducted using a satellite AutoNav software developed by the authors. Detailed data simulation procedures and the verification strategy are presented in this section.

3.1. Ephemerides simulation and verification

Due to frequent satellite maneuvers, we cannot obtain continuous ephemerides for all the satellites in six months to simulate ISL observations without interruption. 21 GPS satellites with continuous ephemerides of 181 days since Jul 2, 2015, were chosen to represent MEOs of BDS; Beidou GEOs and IGSOs are maneuvered at such a high frequency, about 12 times and twice for each GEO and IGSO each year, respectively [37], that continuous ephemerides of half a year are not available. We used IGS precise ephemerides for the 21 MEO satellites and simulated ephemerides for the GEOs/IGSOs based on the available precise ephemerides. A constellation of 21 MEOs, 5 GEOs, and 5 IGSOs was considered in this experiment. The 21 MEOs are distributed on 6 planes with inclination angles of approximately 55°, the 5 IGSOs are on 3 planes with similar inclination angles to those of MEOs, and their distribution is illustrated in Figure 2. It should be noted that the PRNs of GEOs/IGSOs are consistent with their actual ones in BDS; for MEOs, the PRNs are the actual GPS PRNs added by ten. Although the satellite configuration is not entirely the same as the future BDS, it can serve the purpose of this study.

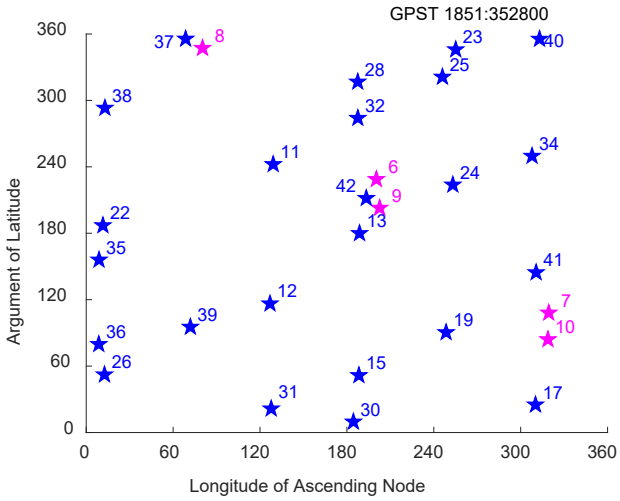

Fig. 2. Distribution of the IGSOs and MEOs

Continuous ephemerides of GEOs/IGSOs were obtained by orbit integration considering the main perturbations. To simulate ephemerides close to reality, with other dynamical forces accurately modeled, the SRP forces of each satellite need to be provided. Firstly, orbit fitting was done with the precise ephemerides of 181 days starting on July 2, 2015, using the Least Squares Method (LSM), and satellite initial position, velocity and 9 SRP parameters of ECOM [16] were estimated daily. Then, orbit integration could be carried out with these estimated initial parameters, and SRP forces for each satellite were calculated with intervals of 300 s in orbit integration process using satellite position and velocity of each epoch, as well as the SRP parameters. For satellites without ephemerides on certain days, SRP forces were calculated by orbit integration with initial values from the previous day, which solved the problem of the lacking ephemerides due to maneuvers. Finally, satellite ephemerides were simulated with these modeled SRP forces and other perturbation models by orbit integration starting from July 2, 2015 using the estimated initial orbit parameters. The reference frames and dynamic models adopted in this process are the same as those used in AutoNav (Table 2), except the SRP model. Satellite clock errors were from the IGS clock products of BDS and GPS.

In order to validate the feasibility of using simulated ephemerides for GEOs/IGSOs to generate ISLs, AutoNav for the constellation with only 21 MEOs has been firstly conducted with ISL observations generated from the real and simulated ephemerides, respectively. The real ephemerides are the IGS precise orbit products, and the simulated ones are generated in the same way as the simulated ephemerides of GEOs/IGSOs. The simulation conditions of these MEO crosslink observations and the corresponding observation errors and noises are the same as those for the whole BDS constellation, illustrated in the following subsection. The AutoNav performance was evaluated by comparing the estimated satellite orbits and

clocks with true values, which were used for crosslink observation generation. The AutoNav system ensemble clock has a bias from UTC, which has an effect on timing for the users; only the relative clock errors affect the calculated ranges between the receiver and satellite and thus affect user positioning accuracy. The RMS errors of the whole constellation in orbit radial and horizontal directions are expressed as RERR and PERR, and CERR for the relative clock errors, as defined in the literature [4]. AutoNav orbit RMS errors of the purely MEO constellation in the radial and horizontal directions are shown in Figure 3. It can be seen that the RERR keeps within 1.1 m in the first over 100 days and then grow up to 2.0 m in the later epochs for both cases; the PERR has a slow increase in the first over 100 days and grows rapidly to about 34 and 28 m for the cases of real and simulated ephemerides, respectively. The orbit errors of these two situations are comparable, and the orbit accuracy is improved by no more than 18% while using the simulated ephemerides. Therefore, the strategy of using simulated ephemerides for GEOs/IGSOs to make up for the unavailability of continuous real ephemerides is feasible.

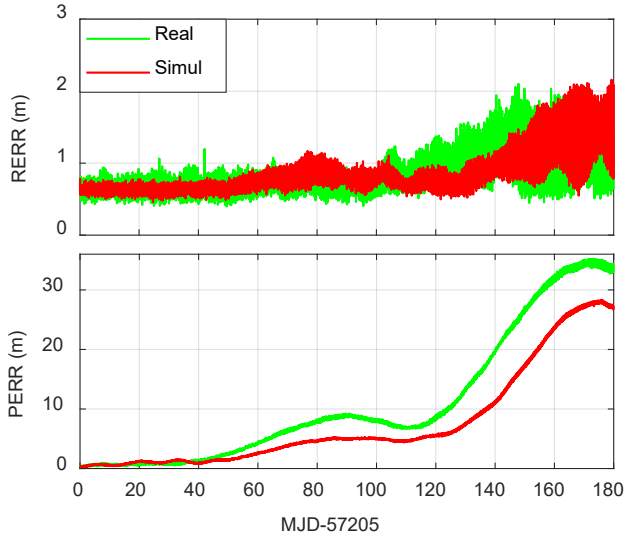

Fig. 3. AutoNav accuracy of MEOs with ISLs generated from real and simulated ephemerides

3.2. ISL simulation

Several conditions have to be satisfied to derive a successful ISL observation: 1. The signal should not be blocked by the earth and be free from the tropospheric effects, and above the ionosphere, if only one frequency data is available; 2. The signal receiving satellite should be within the beam angles of the sending satellite, and similarly, the signal sending satellite should locate within the receiving range of the receiving satellite; 3. Considering the signal strength, the separation between satellites should not exceed a certain distance. The geometry of ISL for satellites SV_i, SV_j is drawn in Figure 4. The angles β_1, β_2 are satellite minimum and maximum beam angle, β is the angle between the line from SV_i to the earth center and the line of sight between two satellites, and H is the distance of the line of sight to the center of the earth. Denote the radius of the earth, the distance of SV_i to the earth center, and the distance between SV_i and SV_j as R, r and D_{ij}. The maximum heights of troposphere, ionosphere, and maximum signal length are H_{trop}, H_{iono} , and L_{max}. The visibility conditions can be expressed as

$$\begin{aligned} & H > H_{trop} + R \quad or \quad H > H_{iono} + R \\ & \beta_1 < \arcsin\frac{H}{r} < \beta_2 \\ & D_{ij} < L_{\max} \end{aligned} \tag{10}$$

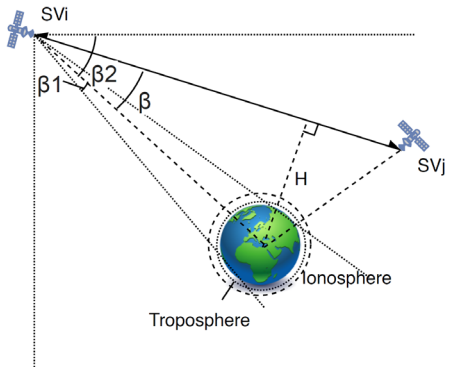

Fig. 4. Geometry of ISL

With a large number of satellites in this experiment, the ISL data could form fairly good observation geometry even only when signals above the ionosphere were used; thus $H_{iono} = 1000km$ was adopted for the first condition. Other condition parameters are given in Table 3.

Table 3 Crosslink pseudo-ranges simulation conditions [27]

Simulation condition	**Value**
GEO/IGSO beam angle and receiving range	$10.0° < \beta < 45°$
MEO beam angle and receiving range	$15.0° < \beta < 60°$
Signal length L_{max}	70000 km

Satellite ISL measurements are affected by different kinds of errors and noises. In this study, errors due to satellite clock biases, relativistic effects, satellite and receiver antenna phase center offsets, and transponder system fixed biases and cyclic variations, and random noises were added to the measurements. Since the quality of the BDS ISL observations is not available, the transmitter and receiver system biases and observation noises were simulated

according to that of GPS Block IIR. The specified crosslink observation accuracy were used for BDS ISL simulation, i.e., 2.5 ns (0.75 m) for both the transmitter bias and its cyclic variation, 4.0 ns (1.2 m) and 3.5 ns (1.05 m) for the receiver bias and cyclic variation, and 2.5 ns (0.75 m) for random noises [38].

The successfully formed ISL measurement pairs are GEO-MEO, IGSO-MEO, and MEO-MEO. The average crosslink pseudo-range pairs (ρ_{ij} and ρ_{ji}) obtained for each satellite in each AutoNav frame during the first week are shown in Figure 5. About 10 satellites are tracking and tracked by each GEO/IGSO satellite and the pair number for each MEO satellite ranges from 16 to 21.

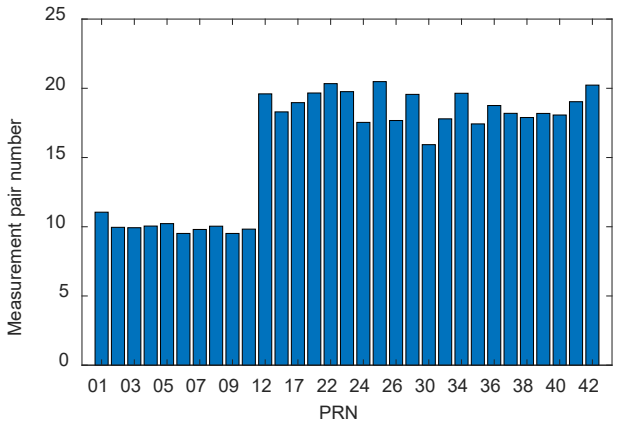

Fig. 5. Average pseudo-range pair number in each frame for each satellite of the first week. Every other satellite PRN is labeled for simplicity

3.3. Accelerometer measurement simulation

SRP and satellite attitude control forces are the main non-conservative perturbations on navigation satellites without the trajectory adjusting maneuver. Based on the analysis in

section 2.2., the influence of attitude control on the accelerometer is not considered in this study. Therefore, SRP should be the primary observables of the onboard accelerometers. The accelerometer data were simulated with the modeled SRP forces as well as the instrument measurement errors, which are relevant to the accelerometer measuring ability. The measurement range and accuracy requirements should be considered while designing an onboard accelerometer.

The SRP forces of a GEO-PRN01, IGSO-PRN06, and MEO-PRN12 on Jul 02, 2015 are plotted in Figure 6. We can see that the SRP forces are on the level of $10^{-7}m/s^2$, and an accelerometer with the range of $\pm 1.5 \times 10^{-7}m/s^2$ can be used for navigation satellites if the maneuver thrust forces are not taken into account. According to the specifications of accelerometers onboard gravity satellites (Table 1), all these accelerometers can satisfy the measurement range requirement. Therefore, we generated the measurement biases according to the accelerometer calibration model (Equation 6 and 7). The scale parameters were assumed to have been accurately calibrated, and thus, scale=1 was adopted in this study; the bias parameters were simulated according to the recommended values of GRACE-A in Table 4. In addition, different levels of white noises were also added into the observation, and the accelerometer accuracy required for AutoNav was investigated.

Table 4 Coefficients of GRACE-A satellite accelerometer biases (Unit:$\mu m/s^2$)

Direction	c_0	c_1	c_2
X-SRF	-1.2095	-4.128E-5	9.7E-9
Y-SRF	29.3370	6.515E-4	-3.9E-7
Z-SRF	-0.5606	-2.352E-6	3.8E-9

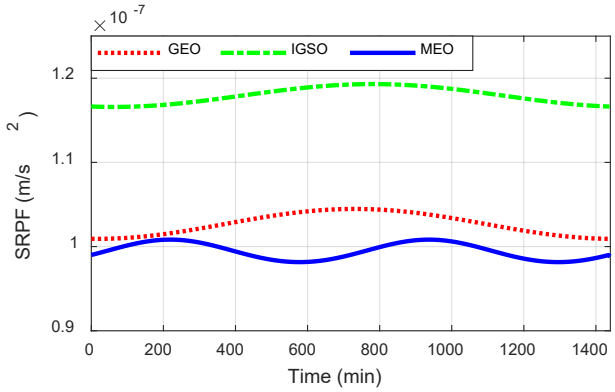

Fig. 6. The SRP forces of navigation satellites. GEO-PRN01, IGSO-PRN06, and MEO-PRN12 on Jul 02, 2015

Figure 7 plots AutoNav orbit accuracies of the BDS constellation when accelerometers of different accuracies were adopted. Orbit RMS errors of the whole constellation in radial and horizontal directions in the 180-day AutoNav period are presented. It is clear that the AutoNav performance improves with the enhancement of the accelerometer accuracy, but not noticeable when the accuracy is increased from $1 \times 10^{-8}\mathrm{m/s^2}$ to $1 \times 10^{-10}\mathrm{m/s^2}$. It may be deduced that with ISL observations of decimeter level accuracy, the satellite accelerometer with an accuracy of better than $\sigma{=}1{\times}10^{-8}m/s^2$ is appropriate for AutoNav. Similarly, with reference to the accelerometer main characteristics (Table 1), we may conclude that the accelerometers onboard CHAMP, GRACE and GOCE can also meet the accuracy requirement of AutoNav. In this study, we simulate accelerometer measurements with the noise of $\sigma = 1 \times 10^{-9}m/s^2$.

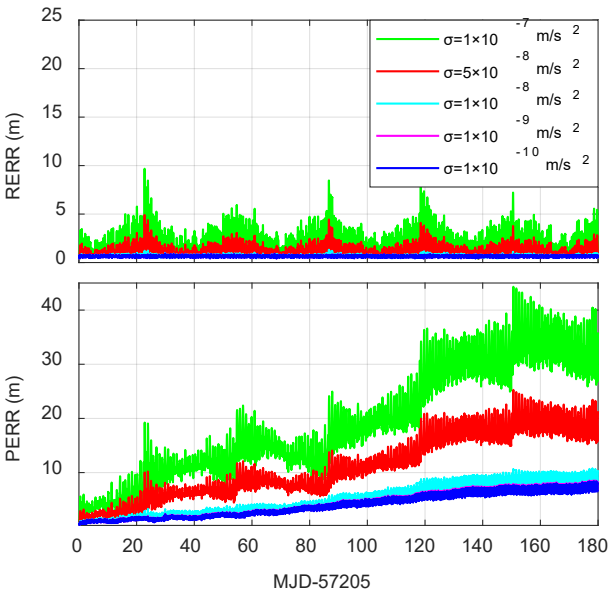

Fig. 7. AutoNav accuracy with accelerometer of different accuracies

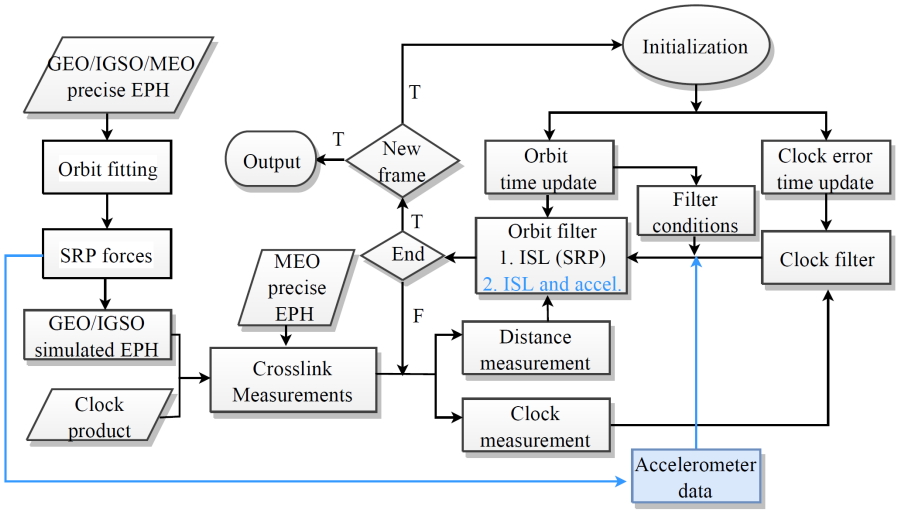

Fig. 8. Flowchart of the AutoNav experiment

4. Results and discussions

Two AutoNav modes are investigated in this paper: using ISL observations only and ISL observations combined with accelerometers. The ISL data were generated from MEO precise

ephemerides and simulated ones of GEOs/IGSOs. Accelerometer data were simulated using the SRP forces estimated from precise ephemerides and measurement errors modeled according to satellite gravity missions.

We first verified the reliability of using simulated ephemerides for GEOs/IGSOs by comparing the AutoNav performance of purely MEOs, with ISL data derived from real and simulated ephemerides, respectively. The comparable results of the two cases indicate that it is feasible to use the simulated ephemerides for GEOs/IGSOs to substitute for the incomplete real ephemerides. AutoNav was subsequently conducted with accelerometers of different accuracies to evaluate the accuracy of accelerometers needed for orbit determination. The results indicate that all the accelerometers onboard CHAMP, GRACE and GOCE satellites may satisfy both the range and accuracy requirements of BDS AutoNav if the maneuver thrust forces are not taken into account.

In this section, the AutoNav accuracies of the two methods are compared, and satellite Keplerian element errors during AutoNav are analyzed.

4.1. AutoNav accuracies with two methods

The AutoNav orbit errors in the radial (dR), along (dA)- and cross-track (dC) directions of the GEO-PRN01, IGSO-PRN06, and MEO-PRN12 while using only ISL observations and ISL combined with accelerometer observations are plotted in Figure 9. In both cases, orbit errors in the radial direction for all the satellites are stable and maintain mostly within ± 1.5 m during the 180-day period, and a tiny improvement can be observed with accelerometers. Both errors in the other two directions increase steadily over time, reaching 15 and 20-25 m in the along- and cross-track component for the GEO/IGSO at the end of 180

days, 5 and 12 m for the MEO. The variation periods of dC correspond to satellite rotation around the earth. While using accelerometer data, orbit errors in the along- and cross-track directions also present slow growth over time, but the magnitudes are much lower. In particular, dA of the GEO, dC of the IGSO and MEO have reduced by half compared to those of the first case.

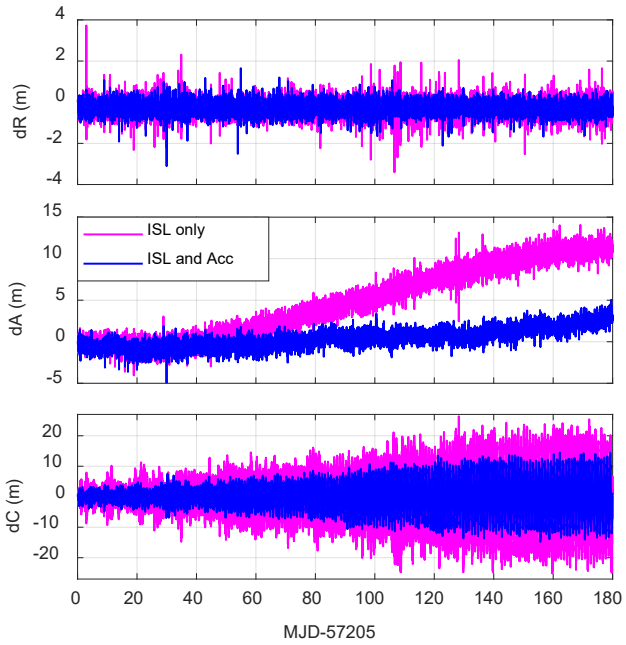

(a) GEO-PRN01

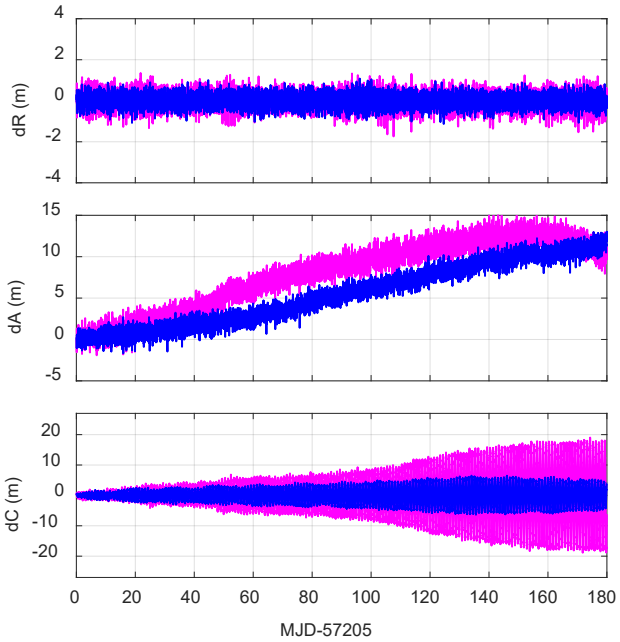

(b) IGSO--PRN06

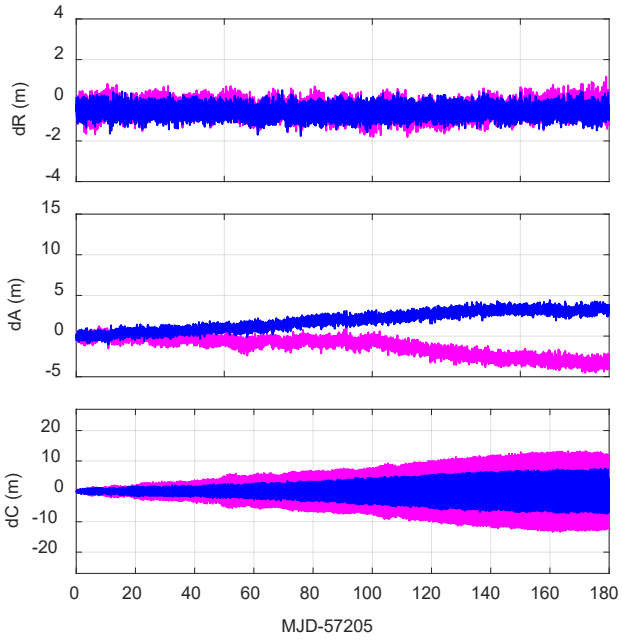

(c) MEO-PRN12

Fig. 9. AutoNav orbit accuracies of the GEO, IGSO, and MEO while using ISL data only and ISL together with accelerometer data

To evaluate the overall AutoNav accuracy, Figure 10 presents the RMS orbit errors in the radial and horizontal directions of all the GEOs, IGSOs, and MEOs in the constellation. It can be seen that the general AutoNav performance of using accelerometers is better than that with only ISL data. RMS orbit errors in the radial direction are relatively steady in both cases but can jump to 2.8 and 1.7 m for GEOs and MEOs in the first case, while keeping within 1.5 and 1.0 m for GEOs and IGSOs/MEOs when accelerometer data are adopted. The horizontal RMS errors have an increasing tendency over time, and the peak points are 12 and 7 m for GEOs/IGSOs and MEOs using accelerometers, which account for just half of the errors when ISL data are used only. We can notice that radial orbit errors of GEOs, IGSOs, and MEOs are quite close, while the horizontal errors of GEOs/IGSOs are nearly twice those of MEOs. This could be explicated by the fact that the satellite orbits in the radial direction are well determined by inter-satellite observations, and the coincident constellation rotation could induce horizontal orbit errors proportional to their altitudes.

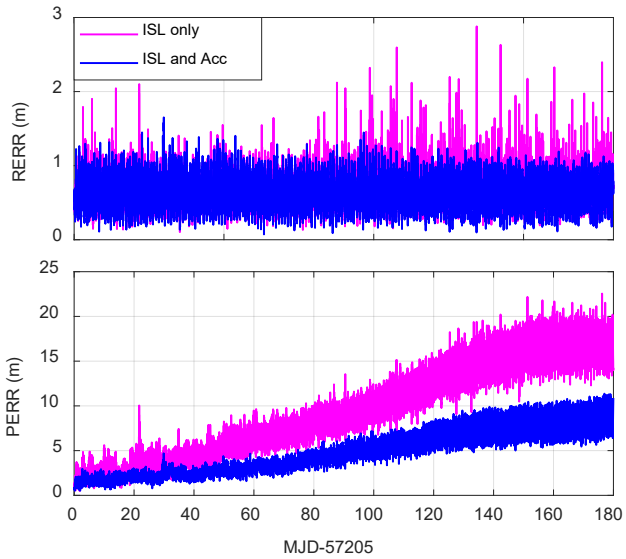

(a) GEOs

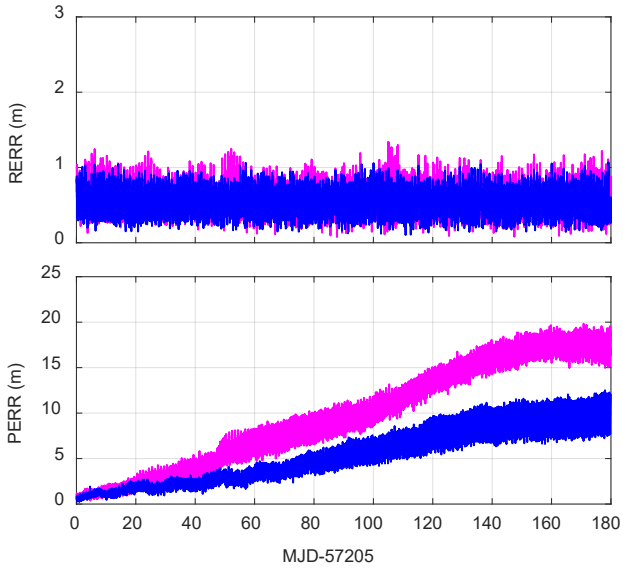

(b) IGSOs

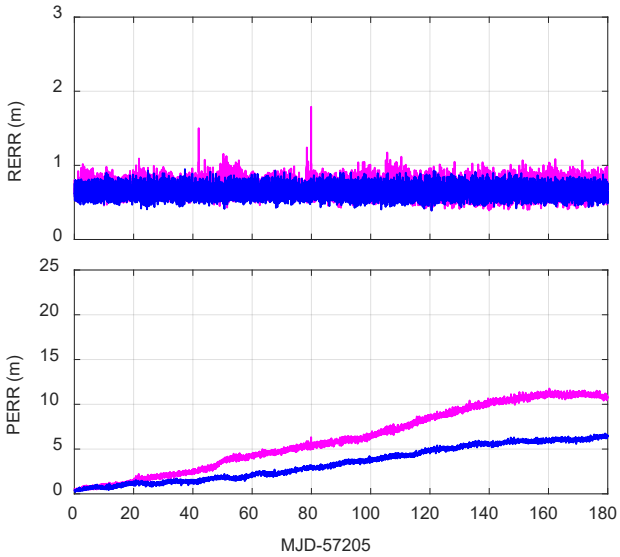

(c) MEOs

Fig. 10. Radial and horizontal orbit RMS errors of GEOs, IGSOs, and MEOs while using ISL data only and ISL together with accelerometer data

As with errors in the radial direction, the relative clock RMS errors also remain at a stable level, less than 0.8 m in the 180-day AutoNav period as can be seen from Figure 11. Also, the clock RMS errors in these two AutoNav cases are almost the same.

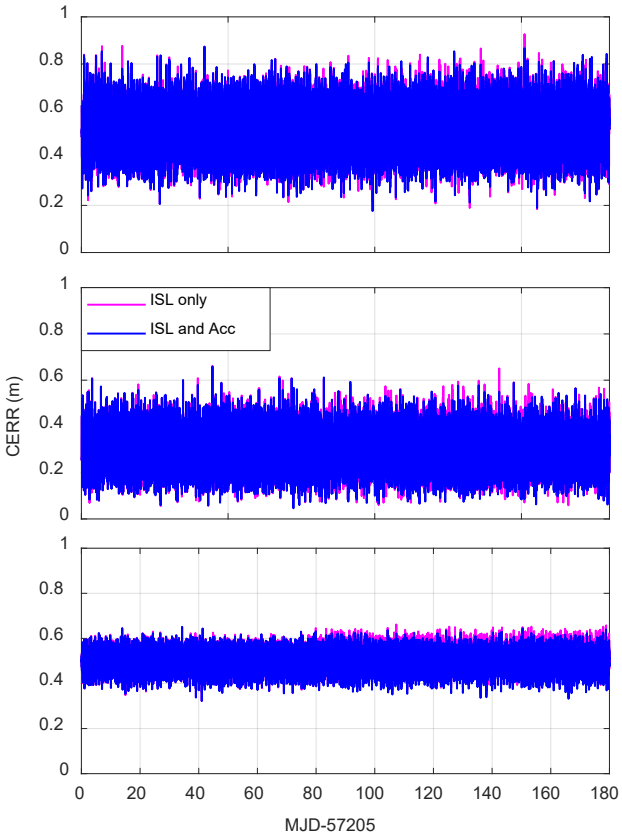

Fig. 11. Relative clock RMS errors of GEOs, IGSOs, and MEOs while using ISL data only and ISL together with accelerometer data. *Top panel*: GEOs, *middle panel*: IGSOs, *bottom panel*: MEOs

4.2. Accuracy of satellite Keplerian elements

To better study the constellation rotation problem, the accuracies of satellite Keplerian elements were also analyzed. Among the ellipse parameters, satellite semi-major axis and eccentricity (a, e) are the ellipse geometric parameters and determine its size and shape. The

orbital inclination and RAAN (i, Ω) represent the vertical and horizontal orientation of the orbital plane; the argument of perigee (ω) defines the orientation of the ellipse inside the orbital plane, the true anomaly (f) indicates satellite position along the ellipse referenced to the perigee, and the argument of latitude $(u = \omega + f)$ illustrates satellite position from the ascending node, which is studied here.

Figure 12 illustrates the errors of the orbital geometric parameter (a, e) of an MEO, PRN12, in two AutoNav cases. The errors in the two AutoNav situations have the same characteristics, varying around zero with nearly constant amplitudes and no increasing tendency with respect to time. The analogous variation patterns are seen for the other two types of satellites, which are not plotted here for simplicity.

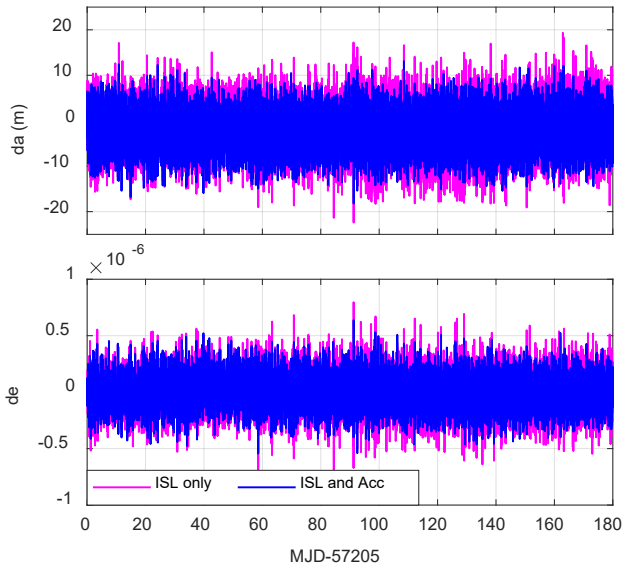

Fig. 12. Geometric parameter (a, e) errors of MEO-PRN12 while using ISL data only and ISL together with accelerometer data

The orbital angular parameter errors of GEOs, IGSOs, and MEOs of the same plane are shown in Figure 13. The errors of angular parameters (i, Ω, u) of IGSOs/MEOs and Ω + u of GEOs increase over time in both AutoNav cases. It is clear that the angular parameter errors for satellites of the same plane have the same changing tendency, indicating that satellite orbits of the same plane have the consistent rotation speed with respect to their true orbits. Comparatively speaking, most of the angular element errors are reduced with the aid of accelerometers, especially Ω + u of GEOs, i of IGSOs and u of MEOs. Furthermore, considering the radius of the satellite ellipse, an angle error of $1.0 \times 10^{-6} deg$ can induce about 0.74 and 0.47 m orbit errors for GEOs/IGSOs and MEOs. It can be seen that satellite orbit horizontal errors in Figure 10 are corresponding to the errors contained in the angular elements. In addition, considering the ratios between the radii of satellites and the earth ($R_{GEO/IGSO} \approx 1.6\ R_{MEO} \approx 6.4 R_{earth}$), and the SPS SIS accuracy standard of 2 m orbit induced URE (DoD 2008), the horizontal orbit errors of MEOs and GEOs/IGSOs should be less than 8 and 12.8 m, respectively. Figure 10 indicates that AutoNav accuracies with accelerometers satisfy this standard throughout the 180 days, but only the first 100 days are within the specified level when only ISL observations are used.

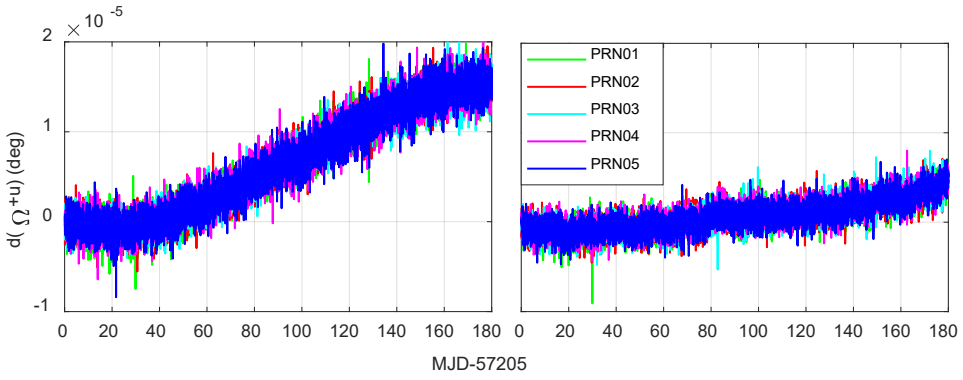

(a) GEOs

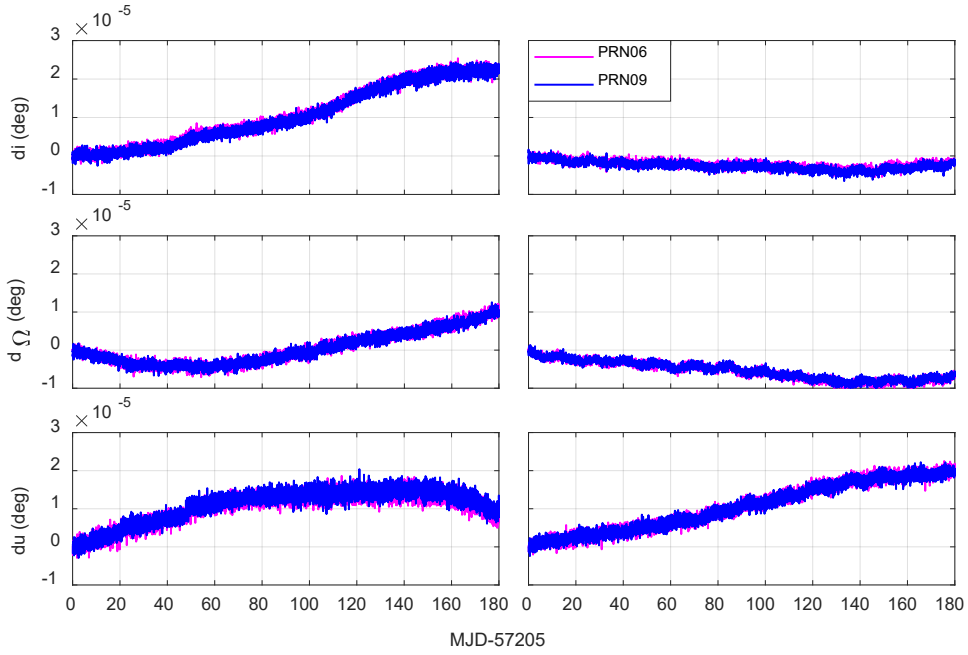

(b) IGSOs

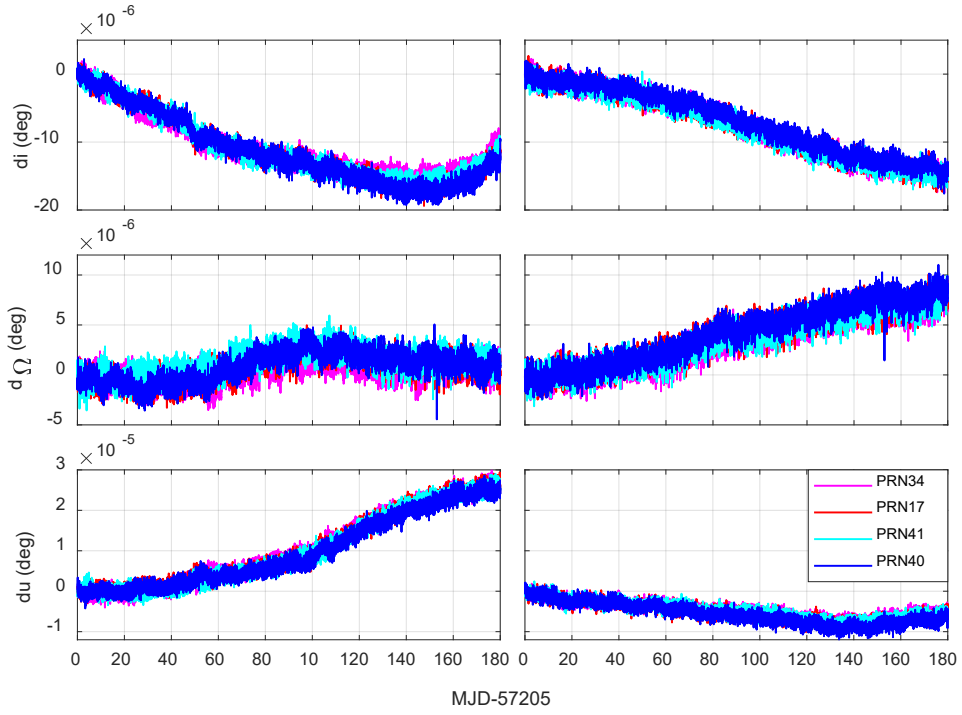

(c) MEOs

Fig. 13. Angular parameter errors for GEOs, IGSOs and MEOs of the same plane. *Left panels*: ISL data only, *right panels*: ISL and accelerometer data

5. Conclusions

The AutoNav system would suffer from the constellation rotation problem due to the lack of absolute measurements and the inaccurate non-conservative force models [11]. Using onboard accelerometers to provide accurate dynamic information in AutoNav mode could be a way to mitigate this problem.

With accelerometers of decent accuracy,$\sigma = 1 \times 10^{-9} m/s^2$, and similar measurement biases to those onboard GRACE satellites, AutoNav has been carried out for BDS during 180 days. The AutoNav accuracy using accelerometers and ISL data has been compared to that of using only ISL data. According to the results, the following conclusions can be drawn.

1. AutoNav performance has been significantly improved by using accelerometers together with ISL data. For better than 2 m positioning error on the earth, orbit accuracy of AutoNav with accelerometers can satisfy this standard throughout its 180-day service period; only the first 100 days can remain within this requirement when only ISL data are used.

2. The constellation rotation can be seen on orbital ellipse parameters. In both AutoNav cases, satellites of the same plane have the similar plane rotation tendency in the horizontal (Ω) and vertical (i) directions as well as the along-track direction (u). The rotation speed can be largely reduced by using onboard accelerometers.

In summary, accelerometers onboard BDS can improve AutoNav accuracy and extend its service span.

6. Future work

In the current study, the frequent maneuvers of Beidou GEO/IGSO satellites are not taken into account.

For the maneuver thrust forces, an adaptive Kalman Filter is a choice to automatically detect maneuver and abandon dynamic models during these periods, only using measurements to calculate satellite position geometrically, and reuse the dynamic information when the maneuver finishes. The maneuvered satellite should be excluded from the AutoNav system once detected and have its orbit determined separately with ISLs and positions of other satellites, and then reincorporated into the system when the orbit returns to normal. As the future BDS has 35 satellites, its overall AutoNav performance can merely be affected due to the loss of an individual maneuvered satellite during some periods.

Additionally, if accelerometers with a measurement range satisfying the amplitudes of thrust forces ($10^{-5} - 10^{-3} m/s^2$) (Qiao and Chen 2018) are implemented onboard, dynamic models can still be used for AutoNav, and successive satellite ephemerides may be derived.

Funding

The work described in this paper was substantially supported by the National Key Research and Development Program of China (Project 2016YFB0502101), and the European Commission / Research Grants Council (RGC) Collaboration Scheme sponsored by the Research Grants Council of Hong Kong Special Administrative Region, China (Project No. E-PolyU 501/16).

References

1. Ananda, M.P., H. Berstein, and R.W. Bruce. *Autonomous Navigation of the Global Positioning System Satelites*. in *AIAA Guidance and Control Conference*. 1984. Seattle, Washington.
2. Codik, A., *Autonomous Navigation of GPS Satellites: A Challenge For The Future.* Navigation, 1985. **32**(3): p. 221-232.
3. Menn, M. *Autonomous navigation for GPS via crosslink ranging*. in *PLANS'86-Position Location and Navigation Symposium*. 1986.
4. Ananda, M.P., et al. *Global Positioning System (GPS) autonomous navigation*. in *Position Location and Navigation Symposium*. 1990. IEEE.
5. Rajan, J.A., M. Orr, and P. Wang. *On-Orbit Validation of GPS IIR Autonomous Navigation*. in *ION 59th Annual Meeting/CIGTF 22nd Guidance Test Symposium*. 2003. Albuquerque, NM.
6. CSNO, *BeiDou Navigation Satellite System Signal In Space Interface Control Document Open Service Signal (Version 2.0)*. 2013, China Satellite Navigation Office.
7. Gong, X., *Parameter integration filter and parameter decomposition filter for Autonomous Navigation of BDS.* GPS Solutions, 2017. **21**(3): p. 1405-1416 DOI: 10.1007/s10291-017-0640-7.
8. Wang, H., et al., *A New Algorithm for Onboard Autonomous Orbit Determination of Navigation Satellites.* Journal of Navigation, 2011. **64**(S1): p. S162-S179 DOI: 10.1017/s0373463311000397.
9. Yang, D., et al., *Globalization highlight: orbit determination using BeiDou inter-satellite ranging measurements.* GPS Solutions, 2017. **21**(3): p. 1395-1404 DOI: 10.1007/s10291-017-0626-5.
10. Bernstein, H., A.F. Bowen, and J.N. Gartside. *GPS User Position Accuracy with Block IIR Autonomous Navigation (Autonav)*. in *Proc. ION GPS 1993*. 1993. Salt Lake City, Utah.
11. Menn, M.D. and H. Bernstein. *Ephemeris observability issues in the Global Positioning System (GPS) autonomous navigation (AUTONAV)*. in *IEEE Position Location and navigation Symposium*. 1994. Las Vegas, Nevada.
12. Rajan, J.A. *Highlights of GPS II-R Autonomous Navigation*. in *Proceedings of the 58th Annual Meeting of the Institute of Navigation and CIGTF 21st Guidance Test Symposium*. 2001.
13. Fliegel, H.F., T.E. Gallini, and E.R. Swift, *Global Positioning System Radiation Force Model for geodetic applications.* Journal of Geophysical Research, 1992. **97**(B1): p. 559 DOI: 10.1029/91jb02564.

14. Ziebart, M. and P. Dare, *Analytical solar radiation pressure modelling for GLONASS using a pixel array.* Journal of Geodesy, 2001. **75**: p. 587-599.
15. Arnold, D., et al., *CODE's new solar radiation pressure model for GNSS orbit determination.* Journal of Geodesy, 2015. **89**(8): p. 775-791 DOI: 10.1007/s00190-015-0814-4.
16. Beutler, G., et al., *Extended orbit modeling techniques at the CODE processing center of the international GPS service for geodynamics (IGS): theory and initial results.* Manuscript Geodaetica, 1994. **19**(6): p. 367-386.
17. Bar-Sever, Y.E. and K. D., *New Empirically Derived Solar Radiation Pressure Model for Global Positioning System Satellites*, in *Interplanetary network progress report*. 2004: Jet Propulsion Laboratory, Pasadena, CA. p. 42-159.
18. Rodriguez-Solano, C.J., U. Hugentobler, and P. Steigenberger, *Adjustable box-wing model for solar radiation pressure impacting GPS satellites.* Advances in Space Research, 2012. **49**(7): p. 1113-1128 DOI: 10.1016/j.asr.2012.01.016.
19. Rajan, J.A., P. Brodie, and H. Rawicz. *Modernizing GPS Autonomous Navigation with Anchor Capability*. in *Proc. ION GPS 2003*. 2003. Oregon Convention Center, Portland, OR.
20. Janschek, K. and S. Dyblenko, *Satellite Autonomous Navigation Based on Image Motion Analysis.* IFAC Proceedings, 2001. **34**(15): p. 111-116.
21. Bruinsma, S., et al., *The impact of accelerometry on CHAMP orbit determination.* Journal of Geodesy, 2003. **77**(1-2): p. 86-93 DOI: 10.1007/s00190-002-0304-3.
22. Bock, H., et al., *GOCE: precise orbit determination for the entire mission.* Journal of Geodesy, 2014. **88**(11): p. 1047-1060 DOI: 10.1007/s00190-014-0742-8.
23. Ash, M.E. *Equipping GPS Satellites with Accelerometers and Satellite-to-Satellite Observables*. in *Proceedings of the 2002 ION National Technical Meeting*. 2002. San Diego, CA.
24. Qiao, J. and W. Chen, *Improving BDS Autonomous Orbit Determination Performance Using Onboard Accelerometers.* Acta Geodaetica et Cartographica Sinica, 2016. **S2** DOI: 10.11947/j.AGCS.2016.F033.
25. Lou, Y., et al., *Precise orbit determination of BeiDou constellation based on BETS and MGEX network.* Sci Rep, 2014. **4**: p. 4692 DOI: 10.1038/srep04692.
26. Zeng, X., *Research and Simulation on Autonomous Orbit Determination for Navigation Satellites*. 2004, Wuhan University: Wuhan
27. Gong, X., *Research on Centralized Autonomous Realtime Orbit Determination and Time Synchronization of BDS*. 2013, Wuhan University.
28. Touboul, P., et al., *Electrostatic accelerometers for the equivalence principle test in space.* Classical and quantum gravity, 1996. **13**(11A): p. A67-A78.

29. Touboul, P., et al. *CHAMP, GRACE, GOCE Instruments and Beyond*. in *IAG Symp*. 2012. Berlin, Heidelberg: Springer DOI: 10.1007/978-3-642-20338-1_26.
30. Frommknecht, B., *Integrated Sensor Analysis of the GRACE Mission*. 2007, Technische Universität München.
31. Dai, X., et al., *Estimating the yaw-attitude of BDS IGSO and MEO satellites.* Journal of Geodesy, 2015. **89**(10): p. 1005-1018 DOI: 10.1007/s00190-015-0829-x.
32. Dilssner, F., *A note on the yaw attitude modeling of BeiDou IGSO-6.* 2017.
33. Bettadpur, S., *Recommendation for a-priori Bias and Scale Parameters for Level-1B ACC Data (Version 2).* GRACE TN-02, 2009.
34. Chen, Q., et al., *An improved GRACE monthly gravity field solution by modeling the non-conservative acceleration and attitude observation errors.* Journal of Geodesy, 2016. **90**(6): p. 503-523 DOI: 10.1007/s00190-016-0889-6.
35. Petit, G. and B. Luzum, *IERS Conventions (2010)*. IERS Technical Note 36. 2010, Verlagdes Bundesamts für Kartographie und Geodäsie, Frankfurt am Main, Germany. 179.
36. Tanizaki, H., *Nonlinear filters: estimation and applications*. 2013: Springer Science & Business Media.
37. Qiao, J. and W. Chen, *Beidou satellite maneuver thrust force estimation for precise orbit determination.* GPS Solutions, 2018. **22**(2) DOI: 10.1007/s10291-018-0705-2.
38. Martoccia, D., et al. *GPS Satellite Timing Performance Using the Autonomous Navigation*. in *Proc. ION GPS 1998*. 1998. Nashville, Tennessee.

Author Biographies

Jing Qiao obtained her PhD degree from the Department of Land Surveying and Geo-Informatics, Hong Kong Polytechnic University in 2018. She received her B.S. degree in Geodesy from Wuhan University in 2013. Her research interests include satellite autonomous navigation, satellite maneuver detection, precise orbit determination, and its application.

Guochang Xu is a professor at Institute of Space Science, Shandong University. He obtained his PhD from the Technical University Berlin in 1992. Having worked as a scientist at the GFZ from 1993 to 1998 and as a senior scientist at the National Survey and Cadastre, Denmark, from 1998 to 1999, he returned to the GFZ as a senior scientist in 1999. He has been a distinguished national expert of Chinese Academy of Space Technology since 2010.

Wanke Liu is currently an associate professor at Wuhan University in China. He obtained his B.S., Master and PhD degrees in Geodesy and Engineering Surveying at the School of Geodesy and Geomatics in Wuhan University in 2001, 2004, and 2008. His main research interests include precise positioning technology of GNSS, autonomous orbit determination of navigation satellites and GNSS/IMU integrated Navigation.

Wu Chen is a professor at Department of Land Surveying and Geo-Informatics, Hong Kong Polytechnic University. Prof Chen has been actively working on GNSS related research for more than 30 years. His main research interests are GNSS positioning quality evaluation, system integrity, various GNSS applications, seamless positioning, and SLAM.